



Available at  
[www.elsevierMathematics.com](http://www.elsevierMathematics.com)  
POWERED BY SCIENCE @ DIRECT•

Journal of Computational and Applied Mathematics 166 (2004) 343–360

JOURNAL OF  
COMPUTATIONAL AND  
APPLIED MATHEMATICS

[www.elsevier.com/locate/cam](http://www.elsevier.com/locate/cam)

# Tensor-product adaptive grids based on coordinate transformations

P.A. Zegeling

*Mathematical Institute, Utrecht University, P.O. Box 80.010, 3508 TA, Utrecht The Netherlands*

Received 4 September 2002; received in revised form 13 June 2003

---

## Abstract

In this paper we discuss a two-dimensional adaptive grid method that is based on a tensor-product approach. Adaptive grids are a commonly used tool for increasing the accuracy and reducing computational costs when solving both partial differential equations (PDEs) and ordinary differential equations. A traditional and widely used form of adaptivity is the concept of equidistribution, which is well-defined and well-understood in one space dimension. The extension of the equidistribution principle to two or three space dimensions, however, is far from trivial and has been the subject of investigation of many researchers during the last decade. Besides the nonsingularity of the transformation that defines the nonuniform adaptive grid, the smoothness of the grid (or transformation) plays an important role as well. We will analyse these properties and illustrate their importance with numerical experiments for a set of time-dependent PDE models with steep moving pulses, fronts, and boundary layers.

© 2003 Elsevier B.V. All rights reserved.

**Keywords:** Method of lines; Adaptive grid refinement; Finite differences; Moving grids; Coordinate transformations

---

## 1. Introduction

Over the years a large number of adaptive grid methods have been proposed for time-dependent partial differential equations (PDE) models. Three *main* strategies of adaptive grid methods can be distinguished, namely, static-regridding methods, moving-grid or dynamic-regridding methods, and  $p$ -refinement methods. In static-regridding methods (denoted by  $h$ -refinement) the location of nodes is fixed. A method of this type adapts the grid by adding nodes where they are necessary and removing them when they are no longer needed. The refinement or de-refinement is controlled by

---

E-mail address: [zegeling@math.uu.nl](mailto:zegeling@math.uu.nl) (P.A. Zegeling).

URL: <http://www.math.uu.nl/people/zegeling>

error estimates or error monitor values (which have no resemblance with the true numerical error). In dynamic-regridding methods (denoted by  $r$ -refinement) nodes are moving continuously in the space-time domain, like in classical Lagrangian methods, and the discretization of the PDE is coupled with the motion of the grid. A third approach, often combined with  $h$ -refinement in finite element methods or implemented in ordinary differential equations (ODE) solvers, is characterized by the term  $p$ -refinement, which indicates the possibility of a variable order of approximation during the calculations.

In this paper, we follow the second approach on a structured grid. One of the most popular techniques in one space dimension is the so-called ‘equidistribution principle’. This method aims at ‘equally’ distributing a relevant quantity, called the ‘weight function’, in order to cluster grid points nonuniformly and to reduce the numerical errors. In two space dimensions this technique is not very well-developed, see however [11,17,1] for some interesting extensions to higher space dimensions. Here, we let the grid be adapted in a tensor-like manner in the two spatial directions. The advantage is that nice properties of the method, such as nonsingularity and smoothness, are preserved in each direction. The adaptive tensor-grid method is based on a semi-discretization of a system of two fourth-order PDEs for the grid variables and is coupled to the physical PDE model re-written in a new co-ordinate system. We use the method-of-lines technique: first we discretize the PDEs in the space direction using a finite-difference approximation, so as to convert the PDE problem into a system of stiff, ordinary differential equations (ODEs) with time as independent variable. The discretization in time of this stiff ODE system then yields the required fully discretized scheme.

Several arguments can be given in favour of adaptive tensor-grids. First, in many problems with boundary layers or models with splitting pulses or rotating peaks there is need for adaptation of the grid, but less need for full-adaptivity, which would complicate the numerical procedure. Second, the proposed tensor-grids are both orthogonal and *smooth*, which has a huge positive effect on the local truncation errors in the nonuniform grid approximations. Note that the smoothness of fully-adaptive meshes may be improved by imposing an additional filter on the mesh, but no theoretical guarantees can be given for success. Moreover, the nonuniform grid remains always undistorted, because the Jacobian of the underlying transformation is positive. Furthermore, tensor-grids are computationally cheaper than fully-adaptive meshes, since the structure of the systems is much simpler. Finally, the ‘topological’ structure of tensor-grids is very natural and well-suited for so-called  $h$ - $r$ -refinement methods, i.e. adaptive methods that combine grid movement and local grid refinement (adding/deleting grid points).

The layout of the paper is as follows. Section 2 is devoted to a description of the equidistribution principle in one space dimension. In Section 3, we present the PDE model, the coordinate transformation and the adaptive grid equations. The tensor-grid approach is enhanced with smoothing in both space and time direction and is defined as the solution of adaptive grid PDEs. Section 4 illustrates the importance of smoothness in terms of the local truncation error and gives a numerical example for a one-dimensional advection equation. Numerical experiments for the two-dimensional tensor-grid are shown in Section 5 for a series of test cases, among others, a ‘whirlpool’ model from meteorology, a parabolic PDE problem describing a rotating cone, and the so-called Gray–Scott model, a reaction–diffusion system from pattern formation. Furthermore, a ‘counterexample’ shows the main drawback of the proposed method. Finally, Section 6 lists the conclusions and presents an outlook to future work.

## 2. The equidistribution principle

The general objective in structured  $r$ -refinement techniques is to find transformations (grids) that map steep solutions in the physical coordinates (waves, pulses, etc.) into milder objects in the computational coordinates which can be treated ‘more easily’ with numerical methods. The advantage is then that we may have good cause to hope to prevent or reduce numerical oscillations near steep fronts or improve the local accuracy without increasing the number of spatial grid points too much. For special PDE models with well-known solution properties explicit transformations may be available to meet this goal. However, for general PDE systems with complicated time-dependent solution behaviour this is hardly possible to accomplish. To overcome this problem in one space dimension, a well-known principle that may be used to define the transformation *implicitly* is described by the so-called equidistribution principle. Equidistribution aims at ‘equally’ distributing a positive ‘weight’, ‘grading’ or ‘monitor’ function  $W$  on a spatial grid. Ideally, this  $W$  represents some measure of the numerical error in the discretization (but this is difficult for general situations, and, if already feasible, not computationally efficient). In other words, we would like to choose or compute a nonuniform adaptive grid  $\{x_i: x_l = x_0 < x_1 < \dots < x_{N-1} < x_N = x_r\}$  such that the contributions to the ‘error’ or some related quantity from each subinterval  $(x_k, x_{k+1})$  are the same. This idea can be worked out in the formula (first, we suppress the time-dependence):

$$\Delta x_i W_i = c, \quad i = 0, \dots, N - 1, \quad x_0 = x_l, \quad x_N = x_r; \quad \Delta x_i := x_{i+1} - x_i. \quad (1)$$

Eq. (1) can also be recognized as a discrete version (using, for instance, the midpoint rule) of

$$\int_{x_i}^{x_{i+1}} W(x) dx = c, \quad i = 0, \dots, N - 1; \quad x_0 = x_l, \quad x_N = x_r.$$

The constant  $c$  is then determined from

$$\int_{x_l}^{x_r} W dx = \int_{x_0}^{x_1} W dx + \int_{x_1}^{x_2} W dx + \dots + \int_{x_{N-1}}^{x_N} W dx = \underbrace{c + c + \dots + c}_{N \text{ times}},$$

giving  $c = (1/N) \int_{x_l}^{x_r} W dx$ . The equidistribution principle becomes

$$\int_{x_i}^{x_{i+1}} W dx = \frac{1}{N} \int_{x_l}^{x_r} W dx, \quad i = 0, \dots, N - 1,$$

which means that the monitor function  $W$  is equally distributed over all subintervals. The simplest way of describing equidistribution is to note that from (1) it follows that grid cells  $\Delta x_i$  are small where  $W_i$  is large, and vice versa, since their product is kept constant. Moreover, Eq. (1) can be interpreted as a discrete (finite difference) approximation of the problem

$$\frac{dx}{d\xi} W(x(\xi)) = c, \quad 0 < \xi < 1; \quad x(0) = x_l, \quad x(1) = x_r. \quad (2)$$

Since  $dx/d\xi = 1/d\xi/dx$ , this is equivalent to

$$\frac{d\xi}{dx} = cW(x), \quad x_l < x < x_r; \quad \xi(x_l) = 0, \quad \xi(x_r) = 1.$$

From this expression we can find an explicit formula for the (inverse) transformation  $\xi(x)$ . Note that

$$1 = \xi(x_r) - \xi(x_l) = \int_{x_l}^{x_r} \frac{d\xi}{dx} dx = c \int_{x_l}^{x_r} W d\bar{x}$$

from which follows  $c = 1/(\int_{x_l}^{x_r} W d\bar{x})$  and thus  $d\xi/dx = W(x)/(\int_{x_l}^{x_r} W d\bar{x})$ . Integrating once gives

$$\xi(x) = \int_{x_l}^x \frac{W(s)}{\int_{x_l}^{x_r} W(\bar{x}) d\bar{x}} ds = \frac{\int_{x_l}^x W(\bar{x}) d\bar{x}}{\int_{x_l}^{x_r} W(\bar{x}) d\bar{x}}.$$

Taking the derivative w.r.t.  $\xi$  of (2) yields the two-point boundary value problem for  $x(\xi)$ :

$$\frac{d}{d\xi} \left[ \frac{dx}{d\xi} W(x(\xi)) \right] = 0, \quad x(0) = x_l, \quad x(1) = x_r. \quad (3)$$

An important issue is the choice of the weight function  $W$ . It may be obvious that there is no general rule for all cases. In literature many different functions have been used for all kinds of situations. For example, in [2,9,12] the popular arc-length monitor  $W = \sqrt{1 + u_x^2}$  is used. Pereyra and Sewell [19] derived estimates for the local truncation error to define the weight function. Already in 1913, Sundman [22] (recently improved in [15]) realized the usefulness of a transformation with  $W = u^{p/q}$  for the three-body ODE system. The curvature monitor  $W = (1 + u_{xx}^{2p})^{1/2p}$  places the grid points in regions of large second-derivatives and is investigated in [4]. As an extension of the arc-length function for the gas dynamics equations in [21] a weight function is proposed that depends on the entropy  $s := p\gamma/\rho$ . Finally, Budd and Piggott [6] derive simple but extremely effective monitor functions, such as  $W = u^{p-1}$ ,  $W = |u|^2$ , or  $W = x^\alpha |u|^\beta |u_x|^\gamma$  for PDE models in which scaling, blow up, or similarity properties should be preserved by the adaptive grid. In [8] it is shown that optimal grids with respect to interpolation errors may be obtained by choosing weight functions that depend on certain powers of the second derivative of the solution. Weight functions within this last class have been discussed and intensively tested in [4]. Their conclusions indicate that, in terms of computational efficiency, the time-stepping process is much more expensive than for methods that use first-order derivatives in the monitor (enhanced with smoothing). This (incomplete) short overview of different weight functions in one-dimension indicates that the choice of the weight function  $W$  depends on the properties of the PDE model and also on the computational aspects of the underlying numerical procedure.

In two space dimensions, however, the situation is even more complicated. Although several authors [11,17,1] have described new interesting ideas that all lead in some sense to equidistribution, when restricting the respective method to one space dimension, the theory behind these higher-dimensional versions is far from understood. In the following section, a simplified tensor-grid approach is proposed that yields equidistribution in each spatial direction with additional smoothness properties. This method can be used for models with sharp transitions in the solution, for example in boundary layers or rotating pulses.

### 3. Tensor-product adaptive grids

Consider now the two-dimensional time-dependent PDE model

$$\partial_t u = \varepsilon \Delta u - \beta(u, x, y, t) \cdot \nabla u + s(u, x, y, t), \quad (4)$$

where  $(x, y) \in [x_l, x_r] \times [y_l, y_u]$ ,  $t \in [0, T]$ ,  $0 \leq \varepsilon$  is the diffusion coefficient,  $\beta$  the velocity vector and  $s$  a nonlinear sourceterm.

It is common and useful in structured  $r$ -refinement methods to first apply a coordinate transformation to the physical PDE model (4). The adaptive grid can then be seen as a uniform discretization of this mapping in the new variables. In this paper we make use of a transformation of variables [26,14] in a dimensionally split approach

$$\xi = \xi(x, t), \quad \eta = \eta(y, t), \quad \theta = t, \quad (5)$$

in which  $(x, y)$  and  $(\xi, \eta) \in [0, 1] \times [0, 1]$  denote the physical and computational coordinates, respectively. Applying this transformation to Eq. (4) gives (a similar derivation can be made for a system of PDEs)

$$\begin{aligned} J \partial_\theta u - \partial_\xi u \partial_\eta y \partial_\theta x - \partial_\eta u \partial_\xi x \partial_\theta y &= \varepsilon \left[ \partial_\xi \left( \frac{\partial_\eta y \partial_\xi u}{\partial_\xi x} \right) + \partial_\eta \left( \frac{\partial_\xi x \partial_\eta u}{\partial_\eta y} \right) \right] \\ &- \beta_1 \partial_\eta y \partial_\xi u - \beta_2 \partial_\xi x \partial_\eta u + Js(u, x(\xi, \theta), y(\eta, \theta), \theta), \end{aligned} \quad (6)$$

where  $J := \partial_\xi x \partial_\eta y$  is the Jacobian of the inverse transformation. Note that  $\partial_x \xi = [\partial_\xi x]^{-1}$  and  $\partial_y \eta = [\partial_\eta y]^{-1}$  measure the grid densities in each separate direction.

The adaptive grid in terms of the mapping is determined as a solution of two fourth-order PDEs in  $\xi$  and  $\eta$  with an additional time-dependent component. We set

$$\partial_\xi [(S_1(J_1) + \tau \partial_\theta J_1) W_1] = 0, \quad \partial_\eta [(S_2(J_2) + \tau \partial_\theta J_2) W_2] = 0 \quad (\tau \geq 0), \quad (7)$$

with suitable boundary conditions for  $x$  (similar conditions hold for  $y$ ):

$$x(0, \eta) = x_l, \quad x(1, \eta) = x_r, \quad \partial_n x(0, \eta) = \partial_n x(1, \eta) = 0.$$

The operators  $S_1$  and  $S_2$  are direction-specific versions of the operator  $S$  defined as

$$S = I - \sigma(\sigma + 1)(\Delta\xi)^2 \partial_{\xi\xi}^2 \quad (\sigma \geq 0), \quad (8)$$

where  $J_1 := \partial_\xi x$  and  $J_2 := \partial_\eta y$  are the ‘one-dimensional’ Jacobians, respectively. As mentioned before, several choices for the weight functions in (7) can be made. Here, we simply take

$$W_1 = \sqrt{1 + \alpha \max_y [\partial_x u]^2}, \quad W_2 = \sqrt{1 + \alpha \max_x [\partial_y u]^2} \quad (\alpha \geq 0). \quad (9)$$

The parameter  $\alpha$  is an adaptivity parameter:  $\alpha = 0$  yields  $W_1 = W_2 = 1$  and thus a uniform grid distribution (this can easily be derived from (7) and (8)); for increasing values of  $\alpha$  the derivatives  $\partial_x u$  and  $\partial_y u$  are stressed more and more with the effect of higher spatial grid adaptation. It can be shown that transformation (5) as a solution of Eqs. (7)–(9) satisfies the ‘grid-consistency’ condition

$$J > 0, \quad \forall \theta \geq 0 \text{ and } \forall (\xi, \eta) \in [0, 1] \times [0, 1],$$

and also the ‘local quasi-uniformity’ property

$$\left| \frac{\partial_{\xi\xi}^2 x}{\partial_\xi x} \right| \leq 1/\sqrt{\sigma(\sigma + 1)\Delta\xi}, \quad \left| \frac{\partial_{\eta\eta}^2 y}{\partial_\eta y} \right| \leq 1/\sqrt{\sigma(\sigma + 1)\Delta\eta}. \quad (10)$$

To prove these theoretical properties of the grid, the results from [12] have proved to be very useful. The first property is equivalent to *nonsingularity* of the mapping, which is, of course, a minimum demand. The second property concerns the *smoothness* of the mapping (see below for more details). Note that for  $\sigma = \tau = 0$  (i.e. without smoothing operators) grid equations (7) reduce to

$$\partial_\xi[J_1 W_1] = 0, \quad \partial_\eta[J_2 W_2] = 0, \quad (11)$$

which can be easily solved, just as in the one-dimensional case, to obtain an explicit expression for the (inverse) coordinate transformation

$$\xi(x, t) = \int_{x_l}^x W_1 d\bar{x} / \int_{x_l}^{x_r} W_1 d\bar{x}, \quad \eta(y, t) = \int_{y_l}^y W_2 d\bar{y} / \int_{y_l}^{y_u} W_2 d\bar{y}. \quad (12)$$

Moreover, Eqs. (11) can be seen as the Euler–Lagrange equations of the quadratic ‘grid-energy’ functionals

$$E_1(\xi) = \int_{x_l}^{x_r} \frac{1}{W_1} (\partial_x \xi)^2 dx \quad \text{and} \quad E_2(\eta) = \int_{y_l}^{y_u} \frac{1}{W_2} (\partial_y \eta)^2 dy. \quad (13)$$

Formulae (13) can be taken to represent the energy of a system of springs with spring constants  $W_1$  and  $W_2$  spanning each subinterval (grid points can then be seen as the mass points of the spring system). The grid point distribution resulting from ‘equidistribution’ thus represents the equilibrium state of the spring system, i.e., the state of minimum ‘energy’. Note that, from (11), i.e. without any kind of smoothing, it follows *directly* that, as  $W_1, W_2 > 1$ :  $J_1, J_2 > 0$ , and therefore  $J = J_1 J_2 > 0$ . Using the fact that  $\Delta\xi$  and  $\Delta\eta$  are constant, the continuous property  $J > 0$  both for Eqs. (11) and for Eqs. (7) can be translated in semi-discrete terms as

$$\Delta x_{i,j}(\theta) > 0, \quad \Delta y_{i,j}(\theta) > 0, \quad \forall \theta \in [0, T], \quad \forall i, j. \quad (14)$$

In other words, these relations state that the grid points can never cross one another. Property (10) can be read in semi-discrete terms as

$$\frac{1}{1 + 1/\sigma} \leq \frac{\Delta x_{i+1,j}(\theta)}{\Delta x_{i,j}(\theta)} \leq 1 + 1/\sigma, \quad \forall \theta \in [0, T], \quad \forall i, j \quad (15)$$

and similar relations for the  $y$ -direction. Relation (15) means that the variation in successive grid cells in both directions can be controlled by the parameter  $\sigma$  at every point of time. The importance of this property will be discussed in the next section. Finally, the parameter  $\tau$  in (7) has a smoothing effect in the time-direction to prevent the grid from adjusting too quickly to new values of the weightfunctions  $W_1$  and  $W_2$ . It can be seen as a small delay factor for the grid movement.

#### 4. A numerical experiment in one space dimension

In the previous section, we have shown that the adaptive grid in terms of a coordinate transformation as defined by the solution of PDEs (7) possesses nice properties, such as grid consistency and grid smoothness. In the following, we discuss the backgrounds and effects of the (non)smoothness of the grid and give a numerical illustration in one space dimension to support the theory. An important

quantity in this respect is the so-called ‘grid size ratio’, sometimes also denoted by ‘local stretching factor’. It is defined by

$$r := \frac{x_i - x_{i-1}}{x_{i+1} - x_i} = \frac{\Delta x_{i-1}}{\Delta x_i} := \frac{q}{p}.$$

For the numerical treatment of the physical PDE model we need to approximate spatial derivatives. For instance, the first-order derivatives can be approximated using central-finite-differences:

$$\partial_x u|_i = \frac{u_{i+1} - u_{i-1}}{p + q} + T.$$

The local truncation error  $T$  can be expressed in several different, but mathematically equivalent, ways as follows:

$$\begin{aligned} T &= -\frac{\partial_{xx}^2 u}{2}(1-r)\Delta x_i - \frac{\partial_{xxx}^3 u}{6}(1-r+r^2)\Delta x_i^2 + \dots \\ &= \frac{\Delta \xi^2}{6}(3\partial_{\xi\xi\xi}^3 x \partial_{xx}^2 u + [\partial_{\xi} x]^2 \partial_{xxx}^3 u) + O(\Delta \xi^4) \\ &= \frac{\Delta x_i^2}{6} \left( 3 \frac{\partial_{\xi\xi}^2 x}{[\partial_{\xi} x]^2} \partial_{xx}^2 u + \partial_{xxx}^3 u \right) + H.O.T. \end{aligned}$$

In the case of a uniform grid we have  $r=1$ , and the relation for  $T$  reduces to the standard second-order expression

$$T = -\frac{\Delta \xi^2}{6} \partial_{xxx}^3 u + O(\Delta \xi^4).$$

On the other hand, for  $r > 1$ , i.e. a nonuniform grid, we can derive that the local truncation error will only be of second order

$$\Leftrightarrow r = 1 + O(\Delta x_i), \quad (16)$$

(which is called ‘quasi-uniformity’)

$$\Leftrightarrow \frac{\partial_{\xi\xi}^2 x}{[\partial_{\xi} x]^2} = O(1).$$

A local version of this property is named ‘local quasi-uniformity’ (see also the previous section) and can be expressed as

$$O(1) = \frac{1}{K} \leq r \leq K = O(1). \quad (17)$$

It is easy to make the link between (16) and (17). If we choose  $\sigma = O(1)$  in the smoothed adaptive transformation, then we automatically obtain with  $K := 1 + 1/\sigma : K = O(1)$ . In this sense, the additional smoothing operator gives us the desired property for second-order approximation of the first spatial derivative (note that similar derivations can be made for  $\partial_{xx}^2 u|_i$  and other spatial derivatives appearing in the physical PDE).

Table 1

The maximum error  $\|e\|_\infty$  at  $t = 0.4$  for the one-dimensional-advection model

| $N$  | $\alpha = 0$ | $\alpha = 1, \sigma = 0$ | $\alpha = 1, \sigma = 2$ |
|------|--------------|--------------------------|--------------------------|
| 50   | 0.721312     | 0.624699                 | 0.387192                 |
| 100  | 0.577044     | 0.432729                 | 0.116723                 |
| 200  | 0.509914     | 0.274196                 | 0.033135                 |
| 400  | 0.327693     | 0.142711                 | 0.025296                 |
| 800  | 0.109807     | 0.072737                 | 0.017410                 |
| 1600 | 0.027250     | no solution              | 0.011549                 |

As a numerical illustration we apply a one-dimensional-version of the adaptive grid method defined by (7), where we have frozen the  $y$ -direction, to the following advection model:

$$\partial_t u + 4 \cos(4\pi t) \partial_x u = 0.$$

An exact solution for this problem is given by  $u^*(x, t) = \sin^{1000}(\pi(x - (1/\pi) \sin(4\pi t)))$  and describes an extremely sharp pulse that moves periodically in the time direction from left to right and backwards again through the domain. For the weight function we take the one-dimensional-restriction of (9)

$$W = \sqrt{1 + \alpha[\partial_x u]^2}.$$

Table 1 confirms the theoretical considerations: if we add the smoothing operator ( $\sigma = 2$ ) to the adaptation procedure, the convergence of the method, when doubling the number of spatial grid points, is improved dramatically compared with the uniform grid case ( $\alpha = 0$ ) and with the pure equidistribution case ( $\sigma = 0$ ). In these runs at  $t = 0.4$  the parameters  $\tau$  and  $\text{tol}$  (the tolerance in the time-integrator DASSL [20]) were deliberately chosen very small to see the effect of the spatial part of the smoothing:  $\tau = 10^{-6}$  and  $\text{tol} = 10^{-8}$ . It is observed that the nonsmooth case experiences a severe degradation of performance, even resulting in a breakdown of the method for  $N = 1600$ . The solutions and the grid history for  $N = 100$  are displayed in Figs. 1 and 2. Note the much bigger error in the solution and the ‘unsmooth’ trajectories for  $\sigma = 0$  compared with the plots for  $\sigma = 2$ . It is also clear that the uniform grid solution is far too inaccurate.

## 5. Numerical experiments in two space dimensions

In this section, we will demonstrate the usefulness of the adaptive tensor-grid method in a two-dimensional setting. The method is applied to a set of PDE models from different application areas. In the numerical tests, unless specified otherwise, the default choices in the experiments are the following: a uniform starting grid, a time-tolerance of  $10^{-3}$ , and grid parameters  $\alpha = \sigma = 1, \tau = 10^{-3}$ . For this value of  $\sigma$  the grid cell ratios always remain bounded between  $\frac{1}{2}$  and  $\frac{3}{2}$ . We have discretized the spatial derivatives both in the physical and the adaptive grid PDEs with central finite differences. It is, of course, clear that more suitable approximations, w.r.t. accuracy and efficiency,

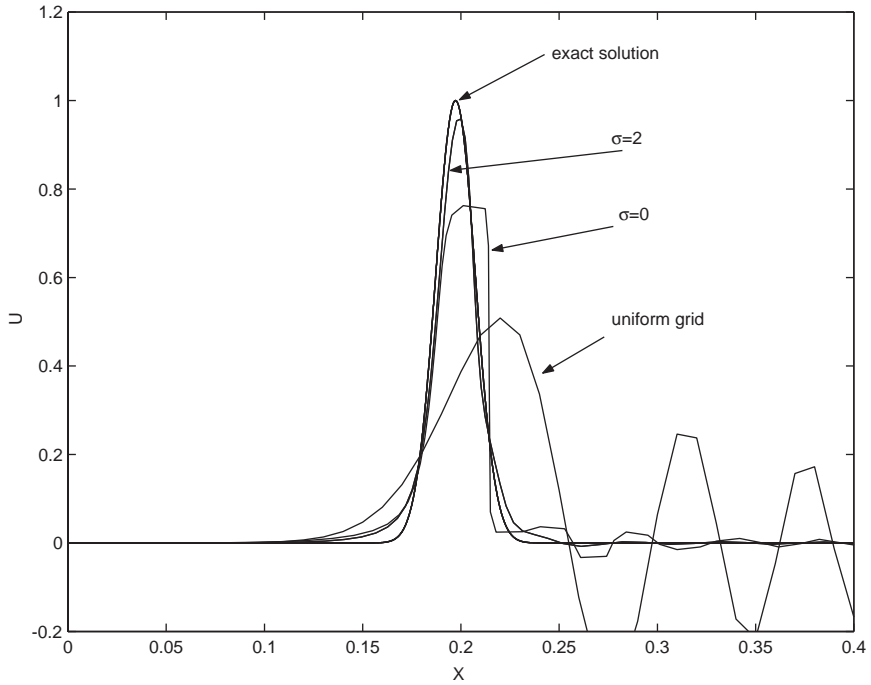


Fig. 1. Numerical solutions for the one-dimensional-advection model for  $N = 100$  at  $t = 4$  for different choices of  $\alpha$  and  $\sigma$  (zoomed in several times around  $x = 0.2$ ).

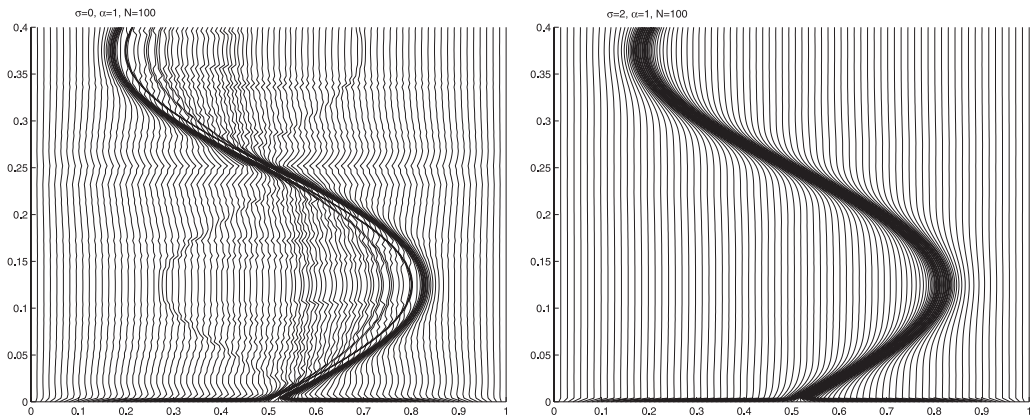


Fig. 2. Numerical results for the one-dimensional-advection model: an irregular adaptive grid for  $\sigma = 0$  (left) vs. a smooth adaptive grid for  $\sigma = 2$  (right).

can be made depending on each separate PDE model. The stiff time-integrator DASSL [20] takes care of the resulting ODE system. This code makes use of  $h-p$ -refinement in the time-direction, which means variable timestep and a variable order (less than or equal 5) of approximation in the backward-differentiation formulas (BDF) integrator.

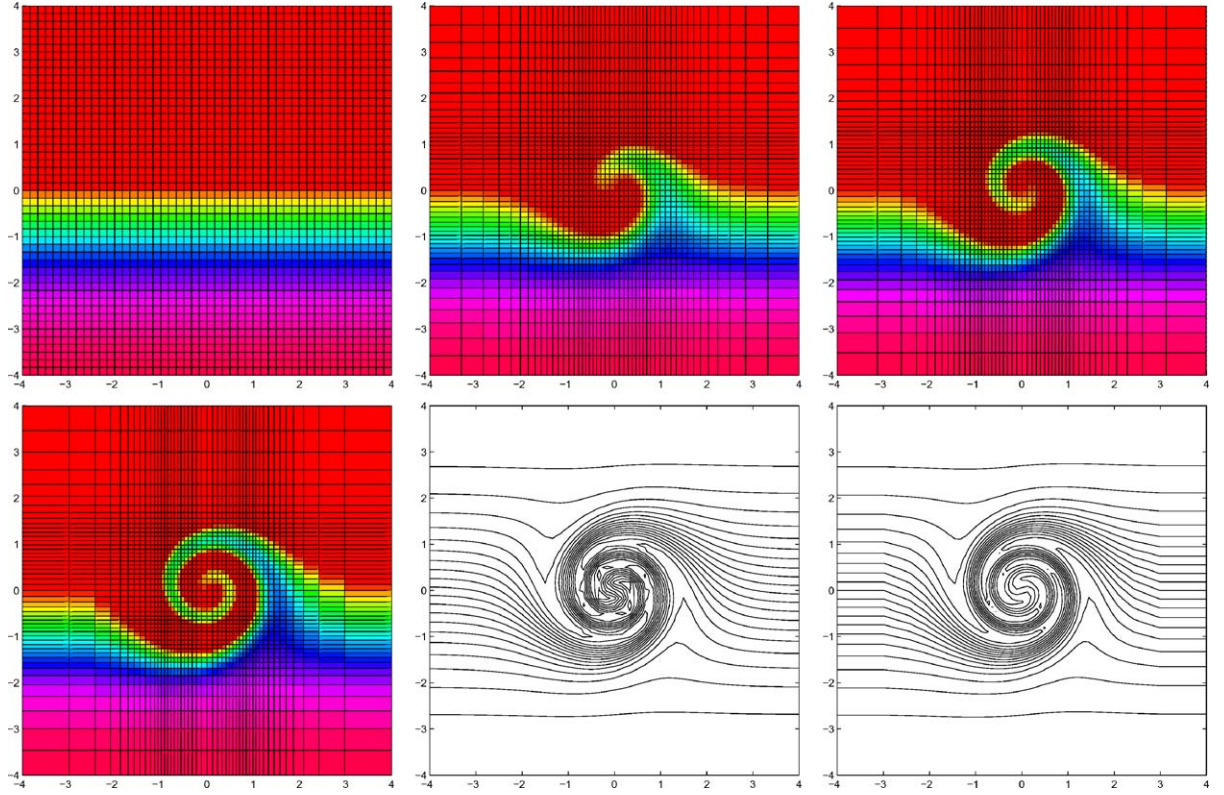


Fig. 3. Tensor-grid solutions for the whirlpool model at  $t = 0.0, 1.6, 2.8, 4.0$  and contourplots at  $t = 4$ : uniform grid vs. adaptive grid (right).

### 5.1. A whirlpool model

An interesting test model from meteorology is described by the hyperbolic PDE

$$\partial_t u = -\frac{v_t}{v_{t,\max}} \frac{y}{r} \partial_x u + \frac{v_t}{v_{t,\max}} \frac{x}{r} \partial_y u, \quad (18)$$

where

$$r = \sqrt{x^2 + y^2}, \quad v_t = \frac{\tanh(r)}{\cosh^2(r)}, \quad v_{t,\max} = 0.385, \quad (19)$$

with initial and boundary conditions:  $u|_{t=0} = -\tanh(\frac{y}{2})$ ,  $\partial_n u|_{\partial\Omega} = 0$ , on the domain  $(x, y) \in [-4, 4] \times [-4, 4]$ ,  $t \in [0, 4]$ . This model describes the formation of cold and warm fronts in a two-dimensional setting. Beginning with a narrow region of high gradients (a front), a fixed (in time) rotational velocity field will act to twist the front in a manner similar to that observed on daily-weather maps (positive solution values correspond to a warm front and negative values to a cold front). Details on this model can be found in [23]. A complicated structure with high spatial activity, similar to a whirlpool, develops in the centre of the domain. Fig. 3 shows the grids and numerical solutions on a  $49 \times 49$  grid at  $t = 0.0, 1.6, 2.8$  and  $4.0$ . Also contour plots are given for comparison with the uniform

Table 2

The maximum error  $\|e\|_\infty$  at  $t = 4.0$  for the whirlpool model

| Grid size | $\alpha = 0$ | $\alpha = 1, \sigma = 0$ | $\alpha = 1, \sigma = 1$ | $\alpha = 10, \sigma = 1$ |
|-----------|--------------|--------------------------|--------------------------|---------------------------|
| 19 × 19   | 0.99983      | 0.57177                  | 0.62015                  | 0.50516                   |
| 29 × 29   | 0.74773      | 0.27647                  | 0.25053                  | 0.24930                   |
| 39 × 39   | 0.52421      | 0.15113                  | 0.15087                  | 0.13512                   |
| 49 × 49   | 0.29419      | 0.10606                  | 0.09828                  | 0.09244                   |
| 59 × 59   | 0.19357      | 0.08476                  | 0.08387                  | 0.07491                   |

grid and the adaptive grid case for  $t = 4.0$  at which point of time the whirlpool has developed. The adaptive solution compares favourably to the uniform solution in which the inner-layer structure of the whirlpool is not resolved very well at all. Note that we haven taken here the re-scaled value  $\alpha=10$  instead of  $\alpha=1$ , since the domain and the solution have larger scales. In Table 2 the maximum error is displayed at the final time for different values of  $\alpha$  and  $\sigma$ . We see that for  $\alpha=\sigma=1$ , which would be a ‘standard’ choice for a unit-square domain and solution values of  $O(1)$ , the method performs not as good as for the re-scaled  $\alpha = 10$  case. The difference between the smooth ( $\sigma = 2$ ) and the nonsmooth ( $\sigma = 0$ ) case is not so profound for this model, because the steep parts of the solution remain concentrated in the centre of the domain for all time.

### 5.2. A combustion model

A reaction–diffusion system (see [13] for more details) of a so-called single one-step reaction of a mixture of two chemicals that stems from combustion theory often gives rise to moving and stationary layers in the solution. A simplified scalar version of this model is defined by

$$\partial_t u = \varepsilon \Delta u + D(1 + \beta - u)e^{-\delta/u}, \quad (20)$$

where  $D = Re^\delta/\beta\delta$  denotes the Damkohler number,  $R$  the reaction rate,  $\delta$  the activation energy, and  $\beta$  the heat release, respectively. As an initial condition we take a sharp nonsymmetric hump

$$u|_{t=0} = 1 + \sin^{50}(\pi x) \sin^{10}(\pi y).$$

Note that smaller values of the diffusion coefficient  $\varepsilon$  yield steeper fronts in the model: we choose  $\varepsilon = 0.1$  which gives rise to very sharp transitions. At the boundary the Dirichlet condition  $u|_{\partial\Omega} = 1$  is imposed. Due to the interaction between diffusion and reaction a moving steep layer is observed that moves quickly to the boundaries and then settles down in a steady state. The other chemical parameters are typical for a standard test model:  $R = 5$ ,  $\beta = 1$  and  $\delta = 20$ . In Fig. 4 the adaptive-grid solutions and the grids are depicted at different points of time on a  $39 \times 39$  tensor-grid. It can be observed that the adaptive grid is nicely situated around the steep moving flame front, from the initial phase up to the boundary layer steady state.

### 5.3. The Gray–Scott model

From pattern formation the following reaction–diffusion system [9,18] exhibits complicated solution behaviour:

$$\partial_t u = 8 \times 10^{-5} \Delta u - uv^2 + 0.02(1 - u), \quad (21)$$

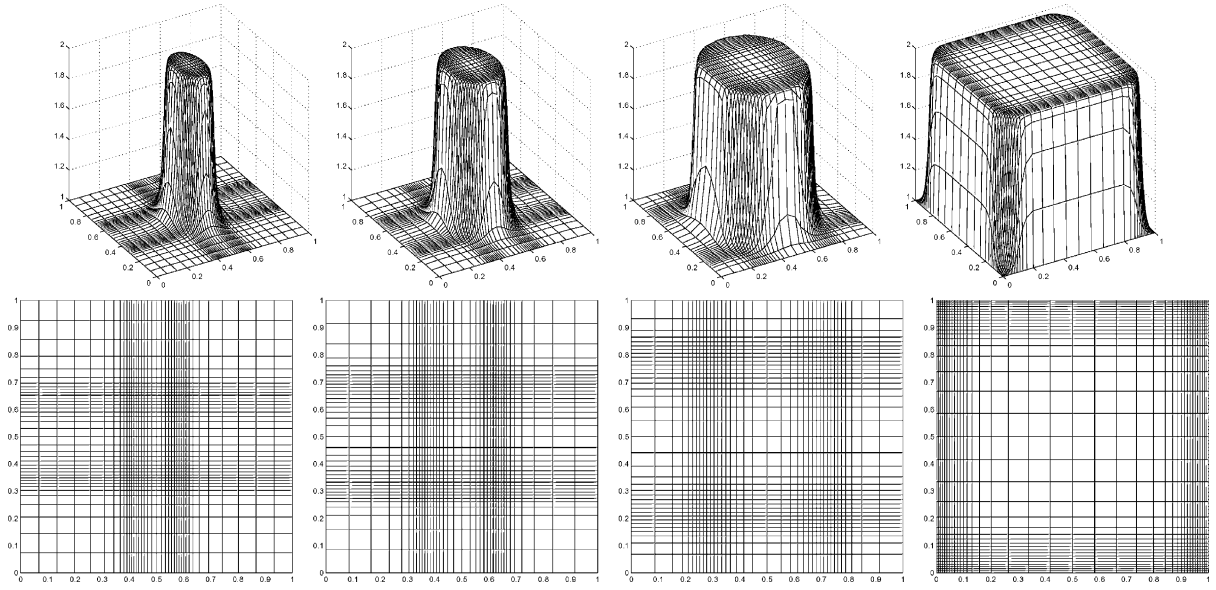


Fig. 4. Tensor-grid solutions for the combustion model at  $t = 0.01, 0.02, 0.04, 0.08$ .

$$\partial_t v = 4 \times 10^{-5} \Delta v + uv^2 - 0.086v. \quad (22)$$

In this model self-replicating spots have been observed. These are regions in which the (chemical) concentrations of some of the species exhibit large amplitude perturbations from a surrounding homogeneous state. Depending on system parameters, these regions can enlarge and split so that the spots replicate in a complex, and as yet incompletely understood, manner. Starting with a pulse, spot, or a small block in the middle of the domain as an initial condition, we see at some point of time that splitting may occur due to a complicated interaction between diffusion and reaction terms, resulting in four spots, later on in eight spots, etcetera. The initial conditions are

$$u(x, y, 0) = \begin{cases} 0.5 & \text{if } 0.45 \leq x \leq 0.55 \text{ and } 0.45 \leq y \leq 0.55, \\ 1 & \text{elsewhere,} \end{cases}$$

$$v(x, y, 0) = \begin{cases} 0.25 & \text{if } 0.45 \leq x \leq 0.55 \text{ and } 0.45 \leq y \leq 0.55, \\ 0 & \text{elsewhere,} \end{cases}$$

on the spatial domain  $[0, 1] \times [0, 1]$ . Note that it would hardly be possible for a uniform grid of moderate size to deal with this tiny initial block. Such a uniform-grid solution could only reproduce the splitting process, which highly depends on derivatives of the solution during the whole time evolution, with a *strong* delay in time and finally also with loosing the symmetry in the solution. This could be repaired by using many uniform-grid points to represent the ‘tiny-block’, but this would be rather inefficient. The adaptive-grid solutions and grids in Fig. 5 demonstrate clearly the capability of the tensor-grid to follow the splitting of the spots. For this experiment, we have used a  $39 \times 39$  grid with endpoint of time  $t = 500$ .

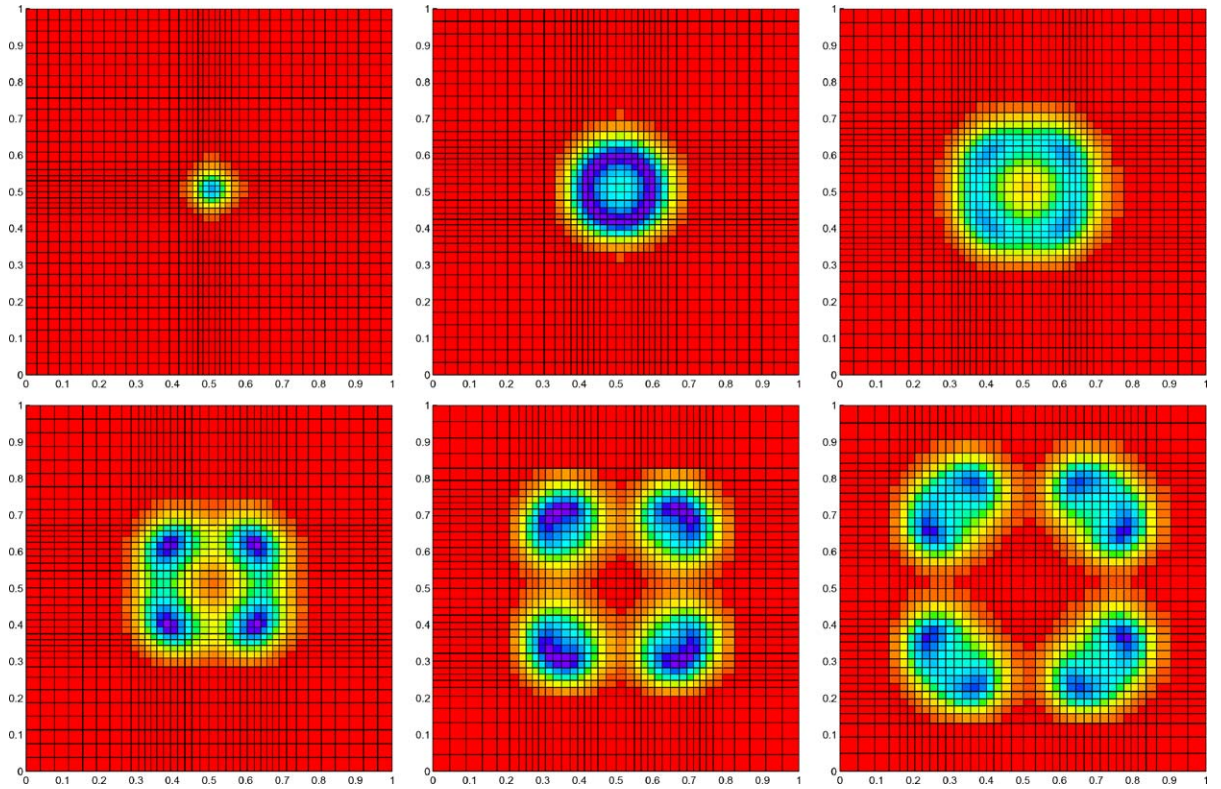


Fig. 5. Tensor-grid solutions for the Gray–Scott model: from initial tiny block at  $t = 0$  (upper-left), via four spots, to eight spots at  $t = 500$ .

#### 5.4. A ‘counterexample’

As we have seen, the proposed tensor-product grid method can be applied successfully to a set of different PDE models in two space dimensions. However, it is also obvious that this method may fail dramatically for a large class of other important models. A relatively simple model that can be used as a ‘counterexample’ (see [25] for details) is given by

$$\partial_t u = \varepsilon \Delta u - u \partial_x u - \left(\frac{3}{2} - u\right) \partial_y u, \quad 0 < \varepsilon \ll 1. \quad (23)$$

The exact solution for this problem reads

$$u^*(x, y, t) = \frac{3}{4} - \frac{1}{4} \frac{1}{1 + e^{(-4x+4y-t+2)/32\varepsilon}}.$$

This is a scalar version of the two-dimensional system of Burgers’ equations. The solution describes a wave front with a steep transition area of thickness  $O(\varepsilon)$  that moves under an angle of  $135^\circ$  with the positive  $x$ -axis. With the adaptive tensor-product grid, the grid points find an ‘optimal’ position at  $t = 2$  as shown in Fig. 6: a uniform grid distribution. Any other choice for the weight function or method parameters yields a preference direction which definitely will not improve the grid distribution, since the solution is a skew wave. It is clear that a skew wave (and many other

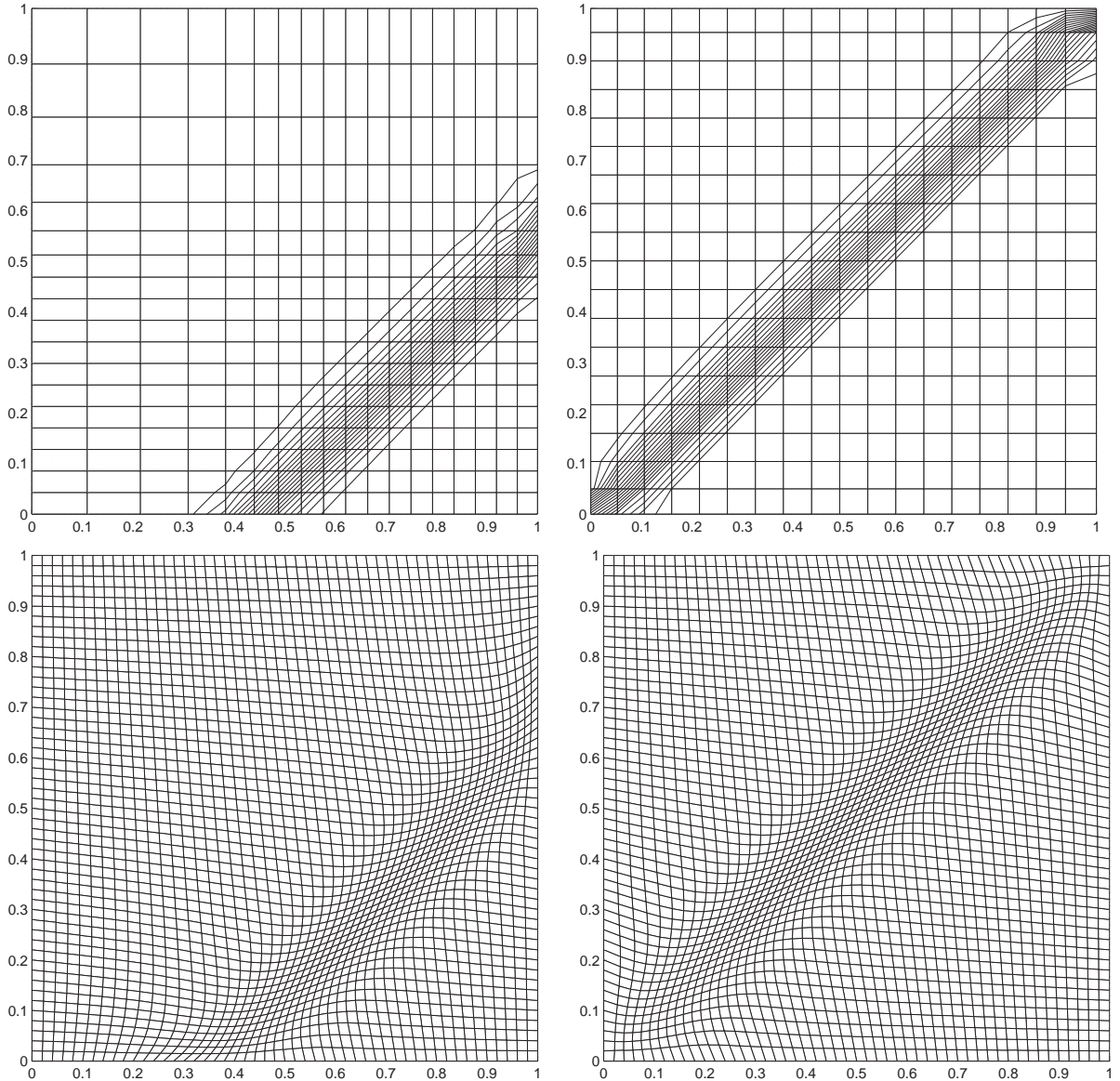


Fig. 6. Tensor-grids with exact contour lines of the solution (upper) compared with fully two-dimensional adaptive grids (lower) for the scalar two-dimensional Burgers' equation at  $t = 0.5$  and  $t = 2$ .

types of more complicated layers than this one) can *not* be resolved with a tensor-product grid. In this figure, we show fully-two-dimensional adaptive grids for this model as well, which are based on the more general transformation  $x(\xi, \eta, \theta)$  and  $y(\xi, \eta, \theta)$ . A description of such a method will appear in a subsequent paper [27]. This example shows clearly that two-dimensional grid adaptation based on the ‘full’ transformation is needed to cope with general solution structures, such as waves and moving layers.

Table 3

The maximum error  $\|e\|_\infty$  at  $t = 2.0$  for the rotating cone model

| Grid size | $\alpha = 0$ | $\alpha = 1, \sigma = 0.2$ | $\alpha = 1, \sigma = 1$ | $\tilde{\alpha} = 1, \sigma = 0$ | $\tilde{\alpha} = 10, \sigma = 0$ |
|-----------|--------------|----------------------------|--------------------------|----------------------------------|-----------------------------------|
| 19 × 19   | 0.43590      | 0.71109                    | 0.11618                  | 0.43998                          | 0.18423                           |
| 29 × 29   | 0.25521      | 0.48283                    | 0.16219                  | 0.26116                          | 0.03766                           |
| 39 × 39   | 0.14363      | 0.21347                    | 0.10206                  | 0.15026                          | 0.02522                           |
| 49 × 49   | 0.08629      | 0.20423                    | 0.08304                  | 0.09600                          | 0.01725                           |
| 59 × 59   | 0.05636      | 0.09953                    | 0.06081                  | 0.06624                          | 0.01147                           |

### 5.5. A rotating cone

To show the effects of the adaptivity parameter  $\alpha$  and the weight function  $W$  it is of interest to examine the linear parabolic equation described by

$$\partial_t u = \Delta u + f(x, y, t), \quad (x, y) \in [-1, 2] \times [-1, 2]. \quad (24)$$

The source term  $f$  is chosen so that the exact solution is

$$u^*(x, y, t) = e^{-80[(x-r(t))^2 + (y-s(t))^2]},$$

where

$$r(t) = \frac{1}{4}(2 + \sin(\pi t)), \quad s(t) = \frac{1}{4}(2 + \cos(\pi t)).$$

This solution is a rotating cone with initial condition  $e^{-80((x-0.5)^2 + (y-0.75)^2)}$  that moves around in circles with a constant speed. During the movement, the shape of the cone does not change. Another option for the weight functions, especially for this example, could be of the form

$$\tilde{W}_1 = \tilde{W}_2 := \sqrt{1 + \tilde{\alpha}u^2},$$

to stress the solution values at the peak itself instead of the gradients. In Table 3 and Fig. 7, numerical results are displayed for different choices of the weight function and the adaptivity parameters  $\alpha$  and  $\tilde{\alpha}$ . A few observations can be made from these simulations. First, we see again, that decreasing the smoothness, i.e., taking the rather small value  $\sigma = 0.2$ , negatively influences the maximum error for the case of an arc-length weight function. Second, the alternative choice  $\tilde{W}_1, \tilde{W}_2$  where the solution value is emphasized, and not the gradient of the solution, gives much better numerical results, although the adaptive grids themselves, perhaps surprisingly, look not too different. Note that, if the value of  $\tilde{\alpha}$  is increased, the error in the numerical solution is reduced significantly. The solutions for  $\alpha = 1$  exhibit a strange decrease in amplitude both at the top of the pulse and at the foot of the pulse, although for  $\sigma = 1$  this behaviour is less pronounced than for the unsmooth run with  $\sigma = 0.2$ . For the alternative weight function with  $\tilde{\alpha} = 10$ , this effect is almost annihilated. This experiment indicates that an optimal choice for the weight function and an optimal value of the adaptivity parameter cannot be given beforehand. This issue needs further attention and will be investigated in a subsequent report.

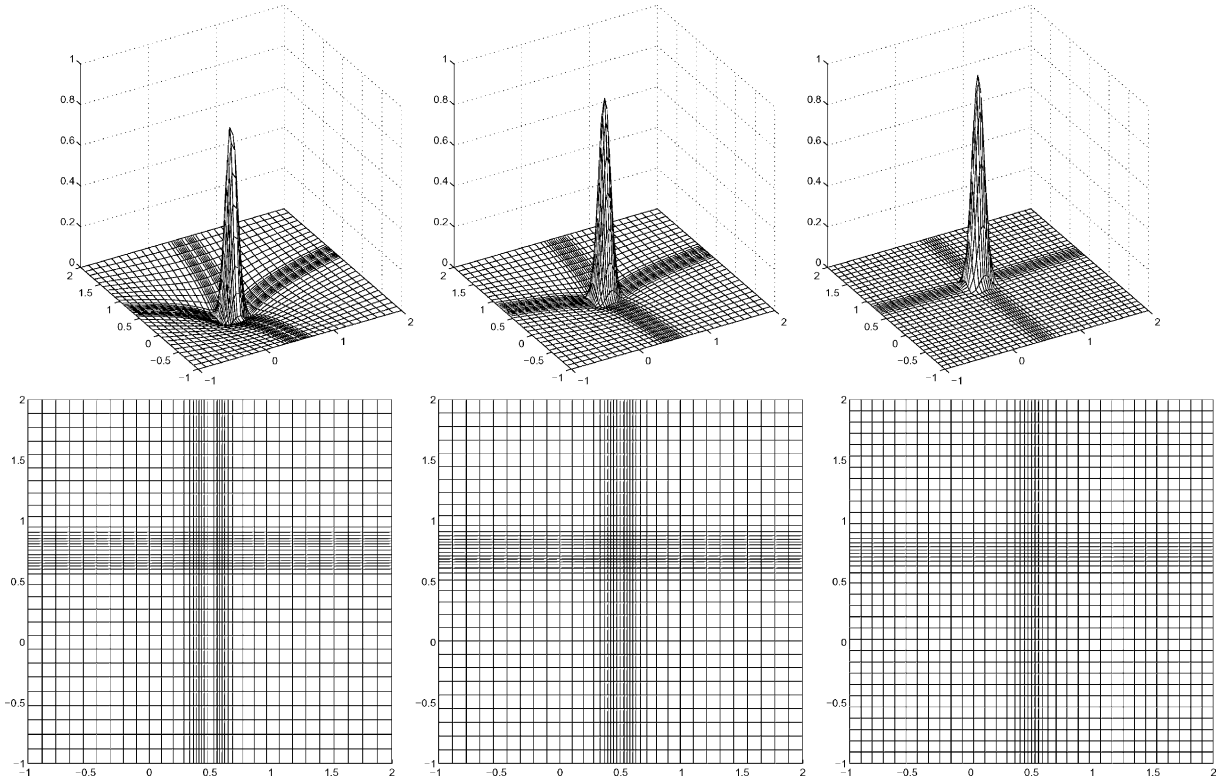


Fig. 7. Tensor-grid solutions for the rotating cone model: solutions and grids after one rotation for, respectively,  $(\alpha, \sigma) = (1, 0.2)$ ,  $(\alpha, \sigma) = (1, 1)$ , and  $(\tilde{\alpha}, \sigma) = (10, 0)$ .

## 6. Conclusions and comments

In this study we have used an adaptive tensor-grid approach for the numerical solution of time-dependent PDE models with steep fronts, rotating or splitting pulses from pattern formation, and boundary layers. The adaptive moving grid used in the experiments is based on the equidistribution principle in two directions enhanced with smoothing operators in the space- as well as in the time-direction. Both theory and experiments in a one-dimensional situation indicated the importance of these additional features of the method. We have shown the effectiveness of the adaptive tensor-grid in two-dimension to deal with regions of high spatial activity in the PDE solution. The main advantage of the proposed method is the fact that nonsingularity and smoothness of the underlying transformation can always be guaranteed, which is one of the known bottlenecks in the theory behind existing structured  $r$ -refinement methods. The method is very useful for solutions with ‘rectangular’ or ‘pulse-like’ steep components moving through the spatial domain. A ‘counterexample’ with a ‘nonrectangular’ wave showed the main handicap of the tensor-grid approach, and indicates the need for full two-dimensional grid-adaptation for these situations (see for example [27]). Another point of discussion is the choice of the weight function. Results were shown for which the traditional choice such as the arc-length weight function is inferior to much simpler functions in which

the solution itself is emphasized instead of the gradients. Further theoretical research is needed to get a deeper understanding of this important issue. Moreover, it is necessary to increase the robustness of the adaptivity parameter in the weight functions. Interesting new developments in this respect can be found in [2], where the parameter is defined as a time-varying constant depending on the volume under the two-dimensional solution surface. Furthermore, in [10] it is claimed that under certain conditions of the nonuniform tensor-grid so-called ‘supra-convergence’ should occur. This higher-order convergence behaviour was not observed in our experiments, however. It could, therefore, be of interest to investigate whether the grid defined by our transformation does or does not satisfy the, rather untransparent, conditions for ‘supra-convergence’. The computational efficiency, especially for more complicated models in two-dimension and three-dimension, can be improved by switching from a direct solver to iterative solvers [5,24] used for the linear systems in the implicit time-integrator. Finally, we note that an efficient combination of the adaptive tensor-grid with a local-uniform grid ( $h$ -)refinement, such as [3], could be of importance for general applications. The effectiveness of  $h$ - $r$ -refinement techniques is demonstrated in [7,16].

## References

- [1] M.J. Baines, Least squares and approximate equidistribution in multidimensions, *Numer. Methods Partial Differential Equations* 15 (1999) 605–615.
- [2] G. Beckett, J.A. Mackenzie, A. Ramage, D.M. Sloan, On the numerical solution of one-dimensional PDEs using adaptive methods based on equidistribution, *J. Comput. Phys.* 167 (2001) 372–392.
- [3] J.G. Blom, R.A. Trompert, J.G. Verwer, Algorithm 758: VLUGR2, A vectorizable adaptive grid solver for PDEs in 2D, *ACM Trans. Math. Software* 22 (1996) 302–328.
- [4] J.G. Blom, J.G. Verwer, On the use of the arclength and curvature monitor in a moving-grid method which is based on the method of lines, Report NM-N8902, CWI, Amsterdam, 1989.
- [5] P.N. Brown, A.C. Hindmarsh, L.R. Petzold, Using Krylov methods in the solution of large-scale differential-algebraic systems, *SIAM J. Sci. Comput.* 15 (1994) 1467–1488.
- [6] C.J. Budd, M.D. Piggott, Geometric integration and its applications, Preprint Department of Mathematics Science, University of Bath, Bath, 2000.
- [7] P.C. Capon, P.K. Jimack, On the adaptive finite element solution of partial differential equations using  $h$ - $r$ -refinement, School of Computer Studies Research Report, 96.13, University of Leeds, Leeds, 1996.
- [8] G.F. Carey, H.T. Dinh, Grading functions and mesh redistribution, *SIAM J. Numer. Anal.* 22 (1985) 1028–1040.
- [9] A. Doelman, T.J. Kaper, P.A. Zegeling, Pattern formation in the one-dimensional Gray–Scott model, *Nonlinearity* 10 (1997) 523–563.
- [10] J.A. Ferreira, On moving finite difference methods for partial differential equations on two-dimensional domains, Preprint 97-10, Dep. de Math., Univ. de Coimbra, Coimbra, 1997.
- [11] W. Huang, Variational mesh adaptation: isotropy and equidistribution, *J. Comput. Phys.* 174 (2001) 903–924.
- [12] W. Huang, R.D. Russell, Analysis of moving mesh partial differential equations with spatial smoothing, *SIAM J. Numer. Anal.* 34 (1997) 1106–1126.
- [13] A.K. Kapila, Asymptotic treatment of chemically reacting systems, Pitman, Boston, 1983.
- [14] P. Knupp, S. Steinberg, Fundamentals of grid generation, CRC-Press, Boca Raton, FL, 1993.
- [15] A. Kvaerno, B. Leimkuhler, A time-reversible, regularized, switching integrator for the N-body problem, *SIAM J. Sci. Comput.* 22 (2000) 1016–1035.
- [16] J. Lang, W. Cao, W. Huang, R.D. Russell, A two-dimensional moving finite element method with local refinement based on a posteriori error estimates, *Appl. Numer. Math.* 46 (2003) 75–94.
- [17] F. Liu, S. Ji, G. Liao, An adaptive grid method and its application to steady Euler flow calculations, *SIAM J. Sci. Comput.* 20 (1998) 811–825.
- [18] J.A. Pearson, Complex patterns in a simple system, *Science* 261 (1993) 189–192.

- [19] V. Pereyra, E.G. Sewell, Mesh selection for discrete solution of boundary problems in ordinary differential equations, *Numer. Math.* 23 (1975) 261–268.
- [20] L.R. Petzold, A description of DASSL: A differential/algebraic system solver, in: R.S. Stepleman, et al. (Eds.), *Scientific Computing, Applications of Mathematics and Computing to the Physical Sciences*, Proc. 10th IMACS World Conference on Systems Simulation and Scientific Computation, North-Holland, Amsterdam, 1983, pp. 65–68.
- [21] J.M. Stockie, J.A. Mackenzie, R.D. Russell, A moving mesh method for one-dimensional hyperbolic conservation laws, *SIAM J. Sci. Comput.* 22 (2001) 1791–1813.
- [22] K.F. Sundman, Mémoire sur le Problème des Trois Corps, *Acta Math.* 36 (1913) 179.
- [23] P. Tamamidis, D.N. Assanis, Evaluation of various high-order-accuracy schemes with and without flux limiters, *Int. J. Numer. Methods Fluids* 16 (1993) 931–948.
- [24] H.A. van der Vorst, Bi-CGSTAB: a fast and smoothly converging variant of Bi-CG for the solution of nonsymmetric linear systems, *SIAM J. Sci. Statist. Comput.* 13 (1992) 631–644.
- [25] P.A. Zegeling, J.G. Blom, A note on the grid movement induced by MFE, *Int. J. Numer. Methods Eng.* 35 (1992) 623–636.
- [26] P.A. Zegeling, R. Keppens, Adaptive MOL for magneto-hydrodynamic PDE models, in: A. Vande Wouwer, Ph. Saucez, W.E. Schiesser (Eds.), *Adaptive Method of Lines*, Chapman & Hall/CRC Press, London/Boca Raton, 2001, pp. 117–137.
- [27] P.A. Zegeling, H.P. Kok, Adaptive moving mesh computations for reaction–diffusion systems, *J. Comput. Appl. Maths.*, 2003, to appear.